

A Non-thermal Study of the Brightest Cluster Galaxy NGC 1275 – The Gamma-Radio Connection Over Four Decades

K. L. Dutson^{1*}, A. C. Edge², J. A. Hinton¹, M. T. Hogan², M. A. Gurwell³ and W. N. Alston^{1,4}

¹*Department of Physics and Astronomy, The University of Leicester, University Road, Leicester, LE1 7RH, UK*

²*Department of Physics, Durham University, South Road, Durham, DH1 3LE, UK*

³*Harvard-Smithsonian Center for Astrophysics, 60 Garden Street, Cambridge, Massachusetts, MA 02138, USA*

⁴*Institute of Astronomy, The University of Cambridge, Madingley Road, Cambridge, CB3 0HA, UK*

Accepted 2014 May 14. Received 2014 May 12; in original form 2014 January 14

ABSTRACT

Emission from the active nucleus in the core of the brightest cluster galaxy of the Perseus cluster, NGC 1275, has varied dramatically over the past four decades. Prompted by the *Fermi* detection of flaring in the γ -ray band, we present the recent increased activity of this source in the context of its past radio and γ -ray output. The broad correspondence between the high-frequency radio data and the high-energy (HE) emission is striking. However, on short timescales this correlation breaks down and the 1.3 mm Submillimeter Array flux is apparently unaffected during *Fermi*-detected flaring activity. The fact that NGC 1275 is also detected at TeV energies during the periods of HE γ -ray flaring suggests that the short-timescale variation might be primarily related to changes in the inverse Compton scattering of photons by the electron population in the jet. The longer-timescale changes suggest a 30–40 year variation in the fuelling of the black hole, that affects the power of the inner jet. NGC 1275 is a laboratory for the class of brightest cluster galaxies, and its variability on these timescales has implications for our understanding of massive galaxies in cooling-core clusters. The case of NGC 1275 highlights the need for wide coverage across the radio band to correctly account for the contribution to emission from a synchrotron self-absorbed core (for example when considering contamination of Sunyaev-Zel’dovich effect observations), and the danger of variability biases in radio surveys of galaxies.

Key words: galaxies: individual: NGC 1275 – galaxies: clusters: individual: Perseus – gamma rays: galaxies – radio continuum: galaxies – radiation mechanisms: non-thermal – galaxies: active

1 INTRODUCTION

The impact of an active galactic nucleus (AGN) on its host galaxy and their wider surroundings was not appreciated until relatively recently (e.g. Bower et al. 2006; Croton et al. 2006). The role of AGN feedback in the formation, evolution, and environment of the most *massive* galaxies is particularly important, given the larger mass of the central black hole and the denser surrounding gas halo of these systems, see McNamara & Nulsen (2012) and Fabian (2012) for recent reviews.

The prototypical example of AGN feedback within a

cluster of galaxies can be found in the Perseus cluster (Böhringer et al. 1993; Fabian 2001), host to the active brightest cluster galaxy (BCG) NGC 1275. The spectral properties of the nuclear narrow-line radio source 3C 84 place it as intermediate between a BL Lac object and a Seyfert galaxy. Significantly, NGC 1275 is one of the very few sources detected by the *Fermi Gamma-ray Space Telescope* (hereafter *Fermi*), that is not strongly beamed (Abdo et al. 2009), and exhibits pronounced flaring activity (see Kataoka et al. 2010; Brown & Adams 2012). During these high-energy (HE) flares, the source becomes significantly harder (Brown & Adams 2012), and bright enough to detect in TeV γ rays (Aleksić et al. 2012). The magnitude of the variability in the HE regime is much greater

* E-mail: kate.dutson@leicester.ac.uk

than that observed in other *Fermi*-detected radio galaxies (e.g. Centaurus-A and M 87). Given this, and given the small sample of such sources, and the fact that NGC 1275 is the most massive of these galaxies, particular attention is warranted.

It has been postulated that the central AGN comprises a viscous accretion disk tilted with respect to the rotating (Kerr) super-massive black hole, bringing about precessing jets as a result of torques acting on the disk (Falceto-Gonçalves et al. 2010). This then accounts for the observed ‘S-shaped’ morphology of the radio jets, which are seen to expand into lobes tens of kiloparsecs in extent. Based on infra-red observations of circumnuclear molecular gas, kinematic arguments imply a black hole mass of $3.4 \times 10^8 M_\odot$ (Wilman et al. 2005). An inherent uncertainty in this value arises from not knowing the system’s true inclination to our line of sight. Very Long Baseline Interferometry (VLBI) maps of 3C 84 can place constraints on this, suggesting that the milli-arcsecond jet is at $\leq 14.4^\circ$ to the observer’s line of sight (Krichbaum et al. 1992). Closer to the core the constraint is more stringent ($\theta \leq 2.7^\circ$), whereas on arcsecond scales the angle is $39.4^\circ \leq \theta \leq 58.2^\circ$. For such conditions to be satisfied, there must be some curvature of the jet away from the line of sight (Dunn et al. 2006). Suzuki et al. (2012) identify new jet components in the core of NGC 1275 from Very Long Baseline Array (VLBA) 43 GHz imaging, that appear between 2002 and late 2008 and show that the majority of the increase in flux density at this frequency is due to the innermost two components. The MAGIC Collaboration et al. (2014) show that for one of these VLBA components (‘C3’), this value almost doubled between the end of 2009 and the start of 2011, which can account for the entirety of the single dish flux increase over this period. Curiously, both Nagai et al. (2010) and Suzuki et al. (2012) claim that C3 is moving relative to C1, as the latter was in the earliest VLBA observations in 2002. However, an alternative interpretation of these observations is that C3 is coincident with the nucleus of the galaxy but was undetected before 2003 due to its inactivity. We will return to this point in Section 4.2. The core is also known to vary significantly on short timescales at optical wavelengths. Kingham & O’Connell (1979) detected variability of in excess of 30 per cent on timescales of months. Similarly, Lyutyi (1977) found variations of 0.2 mag on 10–20 day timescales. Nesterov et al. (1995) show evidence that this optical variability is only observed until 1980.

Observations in the X-ray waveband reveal cavities that anti-correlate with the radio features, leading to the conclusion that the central engine is able, through its jets, to inflate bubbles of hot, relativistic plasma into the surrounding thermal gas of the intracluster medium (ICM), displacing it. Further evidence to support this includes the additional X-ray cavities to the north-west and south of the core, where the the radio lobes have detached and risen buoyantly through the ICM, forming ‘ghost bubbles’. Indeed, the northern bubble has been likened in appearance to a spherical cap air bubble rising in water (Fabian et al. 2003). The position of the older generation of X-ray cavities with respect to the younger, radio-active pair is misaligned, suggesting that the detachment occurred at a different phase in the cycle of jet precession. The observed X-ray and radio emission can be produced by a precession period, τ_{prec} of $3.3 \times 10^7 \text{ yr}$, an

opening angle of 50° , and an inclination of the precession axis to the line of sight of 120° (Dunn et al. 2006).

On larger scales, Perseus hosts a $\sim 300 \text{ kpc}$ radio mini-halo centred on NGC 1275, with spectral steepening away from the cluster core. It has been proposed that the energy required for the particle acceleration is provided by magnetohydrodynamic (MHD) turbulence in the cooling flow (Gitti et al. 2002).

Another feature observed in NGC 1275 is a spectacular optical nebula: a filamentary system of ionised, $\text{H}\alpha$ -emitting gas extending over 100 kpc (Fabian et al. 2003). Both radial and tangential filaments are seen, the latter curving around the galaxy (Conselice et al. 2001), and the brighter features are also detected in the soft X-rays. It has been suggested that they reveal the flow of the hot gas of the rising radio bubbles. An example of such a tracing streamline is the ‘horseshoe’-shaped filament, which clearly turns back on itself at the boundary of the outer buoyant bubble. One interpretation then, is that the bubble draws the ionised gas into its wake as it rises (Fabian et al. 2003), and there is enhanced cooling along its edge, where the ICM is compressed.

The need for a feedback mechanism within the Perseus system to counteract the cooling flow was identified with such measurements as the temperature of intracluster gas, which has been found to be above a third of the virial temperature, given that the ICM has a short cooling time on the galactic scale (Salomé et al. 2006). The coincidence of X-ray cavities with the radio lobes of NGC 1275 is evidence that the central source can suppress gas cooling. Mechanical feedback from the AGN, with an energy output estimated to be $\approx 10^{43} \text{ ergs}^{-1}$, is able to contribute toward this re-heating effect (see e.g. Fabian 1994). Whether some additional source of heating is also necessary to produce the observed suppression is highly debated. Critically, the AGN output of NGC 1275 is variable on decade-long timescales. O’Dea et al. (1984) show that NGC 1275 varied substantially over the 22 years between 1960 and 1982 at 2–100 GHz. Abdo et al. (2009) note that the 15 GHz flux density of NGC 1275 declined dramatically between 1982 and 2005, but has increased steadily since then. They also observe that these changes in radio output are mirrored in the γ rays. It is this connection that we investigate in more detail in this paper.

We begin by describing our analysis procedure in Section 2. Our results are presented in Section 3 and discussed in Section 4, with a focus on the connection between the non-thermal sub-millimetre emission and the gamma radiation, including a review of the historical activity of the source. Conclusions are then drawn and prospects suggested in Section 5.

2 OBSERVATIONS AND DATA ANALYSIS

On board the *Fermi* spacecraft is the Large Area Telescope (LAT): a pair conversion instrument sensitive to high-energy photons ($\sim 20 \text{ MeV} - > 300 \text{ GeV}$) with a large effective area and wide field of view (2.4 sr , and $\sim 6500 \text{ cm}^2$ on-axis at 1 GeV based on post-launch instrument response functions (IRFs), respectively). A detailed description of the detector is given in Atwood et al. (2009) and references therein, and

a post-launch review of its in-flight performance and the IRFs in Ackermann et al. (2012). Primarily, observations are made when the *Fermi* satellite is in *sky survey mode*, i.e. the spacecraft is pointed at some angle from the zenith and rocked about its orbital plane, north for one orbit then south for the next, providing uniform sky exposure on a ~ 3 -hour cycle.

Reprocessed *sky survey mode* event and spacecraft data amassed between the 4th of August 2008 (the date after which science-data-taking began) and the 6th of March 2014 (a Mission-Elapsed-Time interval of 239557417 to 415756803, equating to ~ 2039 days) were extracted for a source region (SR) of 20° centred on the position of NGC 1275 (RA = 49.951° , Dec. = $+41.512^\circ$; taken from data in the literature) and in the energy range $300 \text{ MeV} \leq E \leq 300 \text{ GeV}$, which excludes events at the lowest energies visible to *Fermi*, where the high point spread function (PSF) leads to considerable source confusion. A zenith cut of 100° was applied to exclude HE photons from the Earth's limb, and all 'Source' class events were accepted. The data were analysed using the *Fermi* Science Tools version v9r32p5, and IRF P7REP_SOURCE_V15.

A binned, point-source analysis of NGC 1275 was carried out. Data were fitted to a source model constructed to encompass emission from local (that is, within the SR) sources listed in the *Fermi*-LAT Second Source Catalog (2FGL; Nolan et al. 2012), the diffuse Galactic and extragalactic (isotropic) γ -ray backgrounds (recent models `gll_iem_v05.fits` and `iso_source_v05.txt` respectively¹ were used; their normalisation free to vary) and the candidate source itself. The photon index and normalisation for objects within 1° of NGC 1275 were allowed to vary. Outside of this region but within the specified *region of interest* (ROI) of 10° , the normalisation was free to vary, but the photon index was fixed to the 2FGL value. Sources outside of the ROI but within the SR were included in the model, but both aforementioned parameters were fixed to the catalogue values.

The maximum-likelihood spectral estimator GTLIKE was used to perform a *binned* fit, modelling the source emission with a power law spectrum. GTMODEL was then used to obtain a model map of the region given the result of the fit. GTBIN was utilised to construct a counts map from the data, and a binned exposure cube was generated (through use of the GTEXPCUBE2 tool) as part of the binned likelihood analysis chain. A binned method of likelihood fitting was adopted over an unbinned one, because it has been found to be more robust. The fit outputs a Test Statistic for the source, a spectral index and an integrated flux.

GTBIN was also used to construct source light curves through aperture photometry. Monthly, fortnightly, and 3.5-day binning was applied to the data, within an ROI of 1° . The background was estimated in two manners: firstly, the model-predicted source flux contained therein was subtracted from the overall model-predicted flux, calculated by integrating over the ROI in the corresponding model map given weighted exposure maps across thirty bins in energy. This value was then multiplied by a correction factor to account for the tails of the PSF that lie outside the aperture

selected for the light curve, which was estimated by taking the ratio of the average exposure across all time bins for the light curve-specific ROI and the larger region used to perform the likelihood fit, calculated using the GTEXPOSURE tool. Secondly a 'mean background' light curve was constructed by averaging the flux within a pair of *off-source* regions in the field (at equal Galactic latitudes to NGC 1275, and containing no 2FGL sources) binwise. Subtracting either of these backgrounds from the raw flux in each bin gives an estimate of the relative excess from the source, and allows for comparison between model-dependent and independent measures of the flux level.

The data were divided into two bands in energy (a 'low' cut below 3 GeV, and a 'high' cut above 3 GeV) and the initial analyses repeated in an otherwise identical manner. The ROI selected for constructing light curves in these bands was based on the LAT PSF at the lower energy bound (0.4° for the high band; 2.3° for the low band) in an effort to conserve all available source photons. The evolution of hardness ratio (HR) was investigated by dividing the high-band excess flux by that of the low-band, binwise. The HR was also plotted against the monthly source flux across the full energy range.

The historical radio data have been collated from a number of different studies and observatories. The 14.5 GHz University of Michigan Radio Astronomy Observatory (UMRAO) monitoring of NGC 1275 is presented in Abdo et al. (2009) and we refer the reader to this paper and the excellent historical record that the UMRAO project provides for this source (and many others) for the 4.8, 8.0 and 14.5 GHz light curve of NGC 1275. Our emphasis in this work is the higher-frequency (>20 GHz) data where the coverage is less coherent. O'Dea et al. (1984) present the best pre-1980 light curve of NGC 1275, to which we have added the Metsähovi data (Nesterov et al. 1995) at 32–37 GHz and 90 GHz. We also extract photometric points from Schorn et al. (1968), Hobbs et al. (1969), Fogarty et al. (1971), Epstein et al. (1979), Landau et al. (1980), Flett & Henderson (1981, 1983), Barvainis & Predmore (1984), Steppe et al. (1993), Reuter et al. (1997), and Nagai et al. (2012), at both of these frequencies. We include yearly averages of the 85–95 GHz fluxes from Tripp et al. (2011) in the period between 1996–2010, which are a subset of the data presented in that paper.

The flat spectral index of the source at 30–40 GHz means that the differences between 32 and 37 GHz observations are relatively small, and are swamped by the order-of-magnitude change seen over the last 50 years.

Finally, we include Wilkinson Microwave Anisotropy Probe (*WMAP*) and *Planck* 33/30 and 94/100 GHz data, respectively (Wright et al. 2009; Planck Collaboration et al. 2011) to show the most recent fluxes averaged over each of the nine years of the *WMAP* mission (August 2001 to August 2010), and the first 15 months of *Planck* operations (August 2009 to November 2010).

We also make use of 1.3 mm data from the Submillimeter Array (SMA) calibrator monitoring, to provide a more detailed flux comparison since the launch of *Fermi*, as it has the largest number of available datapoints. Gurwell et al. (2007) describe the SMA Phase Calibrator monitoring in detail. NGC 1275/3C 84 has been observed regularly from the start of SMA operations in late 2002 at 1.3 mm and $870 \mu\text{m}$. Save for gaps between March and May each year

¹ <http://fermi.gsfc.nasa.gov/ssc/data/access/lat/BackgroundModels.html>

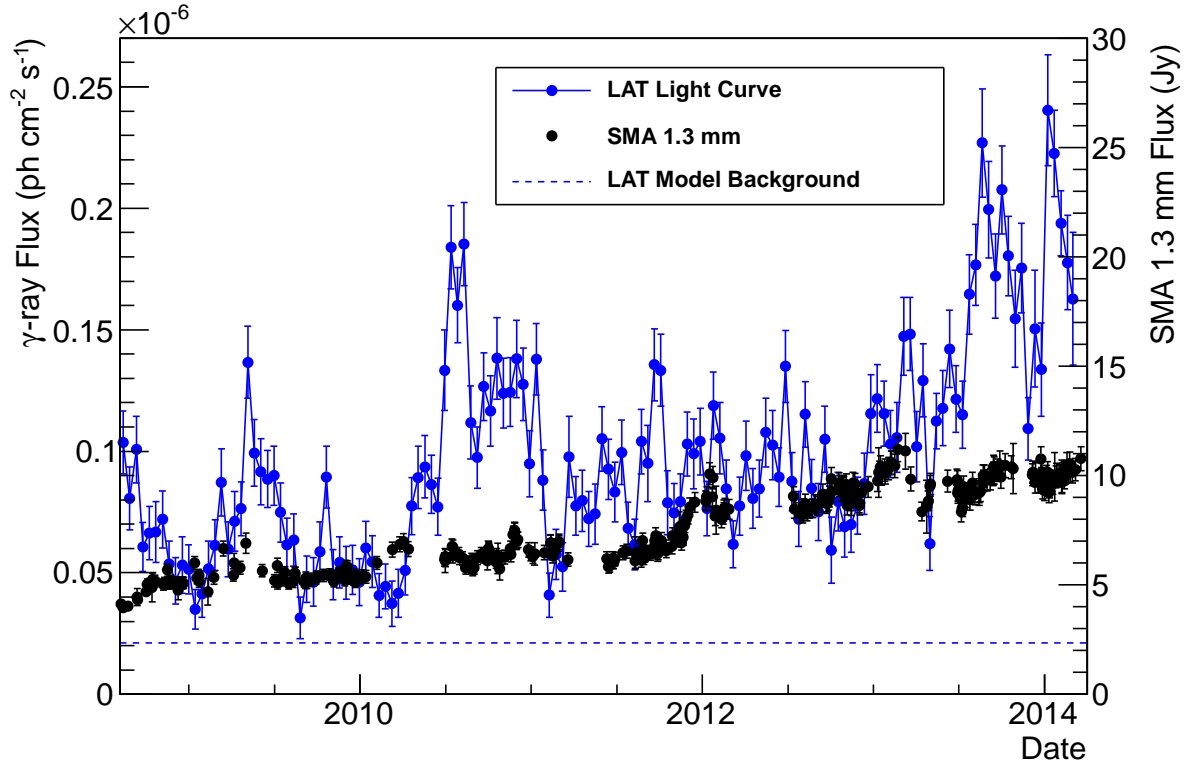


Figure 1. The *Fermi* light curve for NGC 1275 since launch (August 2008), between 300 MeV and 300 GeV and within 1° , with fortnightly binning. The model-predicted background level is indicated, and has been subtracted from the raw flux to produce the source light curve. Overlaid is the SMA calibrator monitoring data at 1.3 mm.

when the source is a daytime object, the time coverage is relatively uniform with typically several observations per week, see Fig. 1. We use all the available data within a frequency range 220–230 GHz to ensure the fluxes are comparable. The SMA observations are made at a variety of baseline configurations, so some flux could be resolved out at the longest baselines. However, given the radio structure at lower frequencies, the fraction of the 1.3 mm continuum that comes from scales larger than $\sim 2''$ is likely to be small even when the source is at its weakest. Therefore the SMA flux should be unaffected by the configuration and any increase can be attributed to flux from the unresolved core component. This selection makes use of over 80 per cent of the 1.3 mm SMA datapoints, as there is a strong preference for this narrow frequency range from SMA observers.

3 RESULTS

The point-source binned likelihood analysis of NGC 1275 between the 4th of August 2008 and the 6th of March 2014 outputs an integrated flux between 300 MeV and 300 GeV of $(7.62 \pm 0.10) \times 10^{-8}$ ph cm $^{-2}$ s $^{-1}$, a photon index of 2.141 ± 0.003 , and a Test Statistic of ~ 27350 (equivalent to a detection significance of $\sim 165\sigma$, see Mattox et al. 1996), where errors are statistical only. Fig. 1 shows the fortnightly-binned *Fermi* light curve for NGC 1275 over this time period, together with the model-predicted background flux within the ROI, and overlaid with the SMA calibrator monitoring

data at 1.3 mm. In the latter, there are several small brightenings (~ 25 –30 per cent) on 1–2 month timescales, but none comparable to the amplitude observed in 1965–1980 as yet. From the *Fermi* light curve, a number of ‘flares’ may be identified, the earliest of which are discussed in Brown & Adams (2012) and Kataoka et al. (2010). An overall trend of increasing baseline flux is seen in both datasets.

Fig. 2 comprises a series of finer (3.5-day binning) *Fermi* light curves for NGC 1275, detailing the 2009–2010, 2010–2012, and 2012–2014 periods (each of which contain prominent flares visible in the fortnightly-binned light curve), and again overlaid with the SMA calibrator monitoring data at 1.3 mm. Though the statistics are poor, these light curves illustrate the erratic nature of the HE flux level, highlighting the differing patterns in each flaring event, and features such as the drop in emission to near-background level in early 2011 (also apparent in Fig. 1).

Fig. 3(a) is a plot of the HR against time with monthly binning, with the source light curve (binned likewise) included for comparison. The possibility of correlation between HR and flux is investigated in Fig. 3(b), which shows the HR plotted against the integrated flux for the full energy range. Observing harder emission during brighter periods is in agreement with Brown & Adams (2012). There is indeed a hint that during the brightest months, the corresponding HR is higher, however this correlation is stronger earlier on, as illustrated by dividing the data into two time periods: In the thirty-five months following launch, the correlation

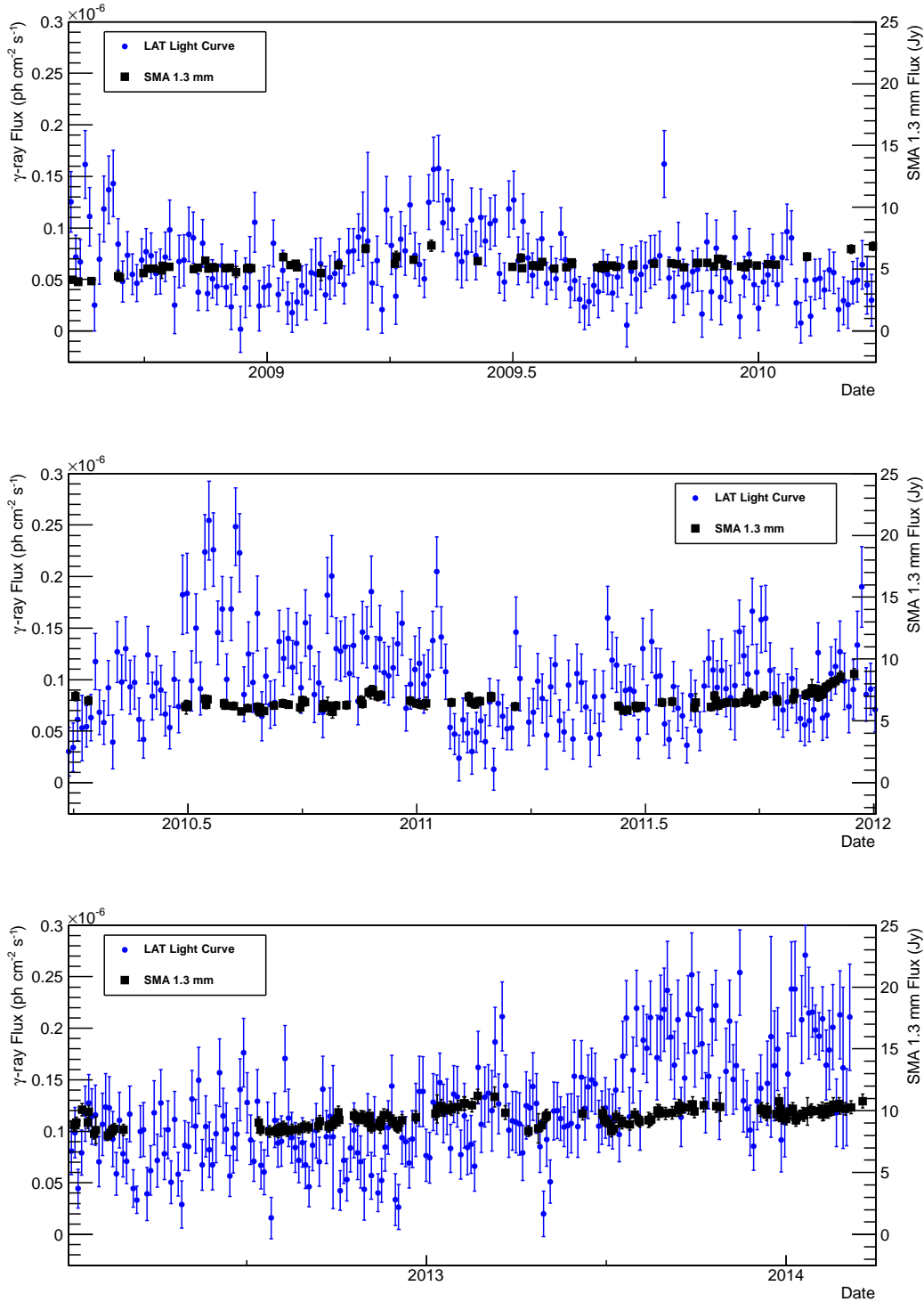


Figure 2. Detailed *Fermi* light curves for NGC 1275, between 300 MeV and 300 GeV and within 1° , focusing on **(top)** the 2009–2010 period, **(middle)** the 2010–2012 period, and **(bottom)** the 2012–2014 period, with 3.5-day binning, overlaid with SMA calibrator monitoring data at 1.3 mm.

factor is 0.53, compared with 0.28 after this epoch, evidencing a deviation from the established *harder-when-brighter* behaviour at later times.

The light curve-specific ROI does contain another point source of HE emission (associated with the radio galaxy

IC 310), and this cannot be easily removed from the light curve, as the emission is barely resolved from that of NGC 1275. The background-subtracted light curve may be very slightly overestimated as a result, but the model, which considers a larger ROI and SR, does include this source.

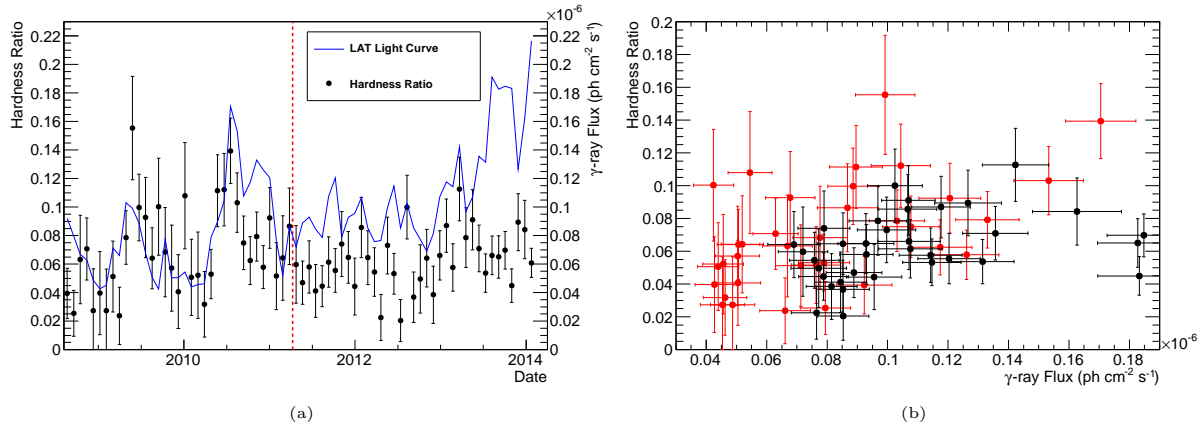


Figure 3. A plot of the hardness ratio (defined in Section 2; derived from ‘high’ and ‘low’-energy band data) against time for NGC 1275, with monthly binning (a), and HR plotted against the γ -ray integrated flux for the full energy range for NGC 1275 (b), with points divided into two time periods: prior to (in red) and following (in black) an apparent increase in the degree of correlation, as indicated by the dashed red line in (a).

Likewise there are several 2FGL sources in the ROI and SR, but these are included in the model. The two methods of background estimation are in agreement within the errors associated with the mean background light curve, which may be fit with a polynomial of order zero, $F_\gamma = (2.50 \pm 0.04) \times 10^{-8} \text{ ph cm}^{-2} \text{ s}^{-1}$, whilst the model-predicted background level is $F_\gamma = 1.21 \times 10^{-8} \text{ ph cm}^{-2} \text{ s}^{-1}$. The choice of background estimate does not very appreciably affect the trend observed in Fig. 3(b). A correlation was sought binwise between the model-subtracted source flux, and the difference between the two background estimates, but not found, rejecting the hypothesis that photons from the PSF tail of NGC 1275 might be contributing significantly to the flux in the off-regions. The model-predicted background was adopted throughout the work presented here, for consistency within the analysis chain. The aperture correction factor applied to this background estimate as described in Section 2 was 1.74 for the overall $300 \text{ MeV} \leq E \leq 300 \text{ GeV}$ band; 1.32 for the high band and 1.25 for the low band.

4 DISCUSSION

4.1 Historical Consideration

Historically, NGC 1275 is a highly-variable source of non-thermal radiation, strongly motivating its investigation with *Fermi*, and particularly suggestive of a relationship between the HE and radio emission. Whilst both leptonic and hadronic scenarios are possible for the γ -ray emission from NGC 1275, we focus in the following on the most common interpretation of this emission as inverse Compton scattering of a relativistic electron population, which is also responsible for the synchrotron emission seen at radio-mm wavelengths.

The European Space Agency (ESA)’s *COS B* mission in the late 1970s (Bignami et al. 1975) revealed an excess of HE emission toward Perseus ($F_\gamma = 8.3 \times 10^{-7} \text{ ph} (> 70 \text{ MeV}) \text{ cm}^{-2} \text{ s}^{-1}$; positional uncertainties were not given), which was interpreted as evidence that NGC 1275 is a γ -ray source (see e.g. Strong & Bignami 1983), however

the galaxy was not detected using the National Aeronautics and Space Administration (NASA)’s Energetic Gamma Ray Experiment Telescope (EGRET) on board the *Compton Gamma-ray Observatory (CGRO)*, which flew throughout the 1990s. A 2σ upper limit for the Perseus cluster of $F_\gamma < 3.72 \times 10^{-8} \text{ ph} (> 100 \text{ MeV}) \text{ cm}^{-2} \text{ s}^{-1}$ was given (Reimer et al. 2003). Contrariwise, NGC 1275 is firmly-detected using the *current-generation Fermi* (Abdo et al. 2009), and in 2010 was detected above 100 GeV using the Major Atmospheric Gamma Imaging Cherenkov (MAGIC) telescopes (Aleksić et al. 2012), establishing the source as a VHE emitter. As noted by Abdo et al. (2009), the γ -ray variability of the source matches that of the higher-frequency radio emission from the UMRAO 15 GHz monitoring. We extend this analysis to 30 and 90 GHz over the past ~ 50 years, and find that the long-timescale variation of both the γ -ray and millimetre emission are related. As shown in Fig. 1 the connection between these two components on shorter timescales is not as well-correlated, but this is to be expected if the millimetre emission is strongly synchrotron self-absorbed early in any flaring event.

Combining all of the archival radio data produces 32–37 GHz and 90 GHz light curves that show a dramatic variation over the past ~ 50 years, as seen in Fig. 4. The scatter in photometry at both frequencies before 1978 may in part be due to the difficulty in determining accurate fluxes, but could also be related to a period of enhanced variability, or ‘flickering’, due to larger variations in accretion during outburst. Interestingly, Nesterov et al. (1995) note this period of strong variability in the radio and optical, and speculate that it is related to the structure of the jet. Taking the period in which there is significant optical variability as 1965–1980 (from fig. 1 in Nesterov et al. 1995), the dramatic declines at 90 GHz and then at 35 GHz follow 1–3 and 7–8 years after this, respectively. Given the increasing time lag seen in the data at lower frequencies due to synchrotron self-absorption, it may be that the very gradual decline at $< 100 \text{ GHz}$ is a combination of the many individual components formed before the 1980 brightening at lower

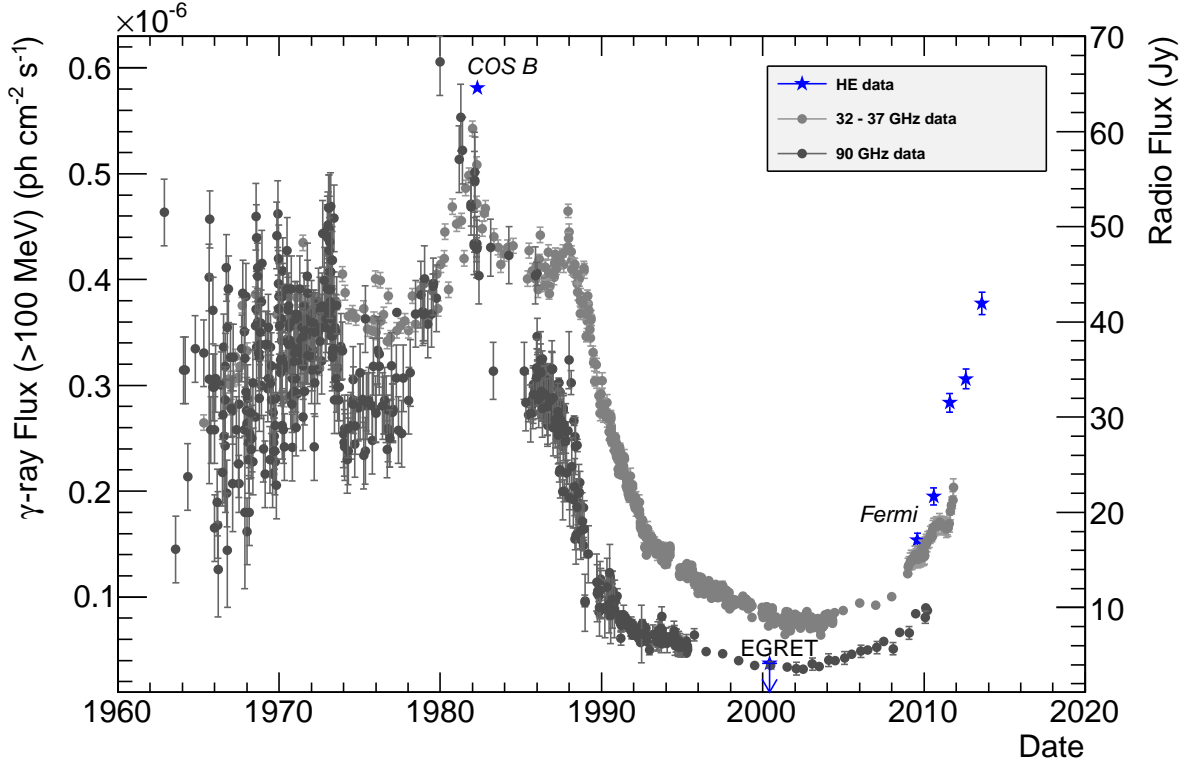


Figure 4. An historical light curve for NGC 1275. A flux above 100 MeV is derived for the emission noted in the *COS B* data in the direction of the cluster. The EGRET upper limit on the flux from Perseus is included, and yearly fluxes for NGC 1275 as observed using the *Fermi*-LAT. Collected archival radio data (described in Section 2 above) is also included, at 90 and 32–37 GHz.

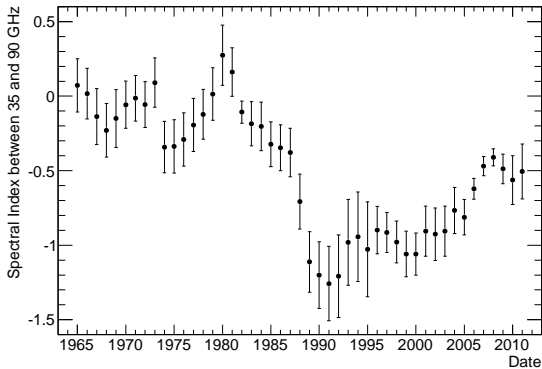


Figure 5. A plot of the average spectral index of NGC 1275, α between 35 and 90 GHz, against time, where the flux is proportional to ν^α

frequencies, before fading as they move away from the core and become less self-absorbed.

We have determined the average spectral index between 35 and 90 GHz for the period during which the two high frequency light curves overlap, and show in Fig. 5 how this spectral index changes over time. The dramatic transition between the period prior to 1980, and the 1990–2000 interval, where the spectral index falls from 0.0 to -1.0, is strongly suggestive of a cessation of activity in the core around 1980,

in line with the aforementioned lack of significant optical variability after that point. The timescale for this change in spectral index is related to the strength of the synchrotron self-absorption at different frequencies.

Fig. 6 shows the yearly-averaged *WMAP* and *Planck* light curves for the source, and the radio-to-far-infrared spectral energy distribution (SED) for 2002 and 2010, including points from the UMRAO monitoring (Aller et al. 1985), and the literature, to show the spectral variation at high frequencies (>5 GHz) during this period, as the flux begins to rise. In particular, note that the 4.8 GHz UMRAO flux falls between 2002 and 2010 compared to the increase seen at all other frequencies.

4.2 Current Outburst

The increase in high-frequency radio and γ -ray emission from NGC 1275, coupled with the change in the spectral index after ~ 2002 implies that the source has become active again. The two epochs in Fig. 6(b) coincide with a minimum in the radio flux, and a point well into the current outburst, respectively. Importantly, they mark the start of the *WMAP* mission in 2002, and the start of the *Planck* survey in 2009. The well-calibrated photometry, particularly for *Planck*, allows us to determine the spectral index well above the peak induced by the synchrotron self-absorption. The most recent data show that the spectral flattening seen in Fig. 6(b) is related to power law emission that extends into

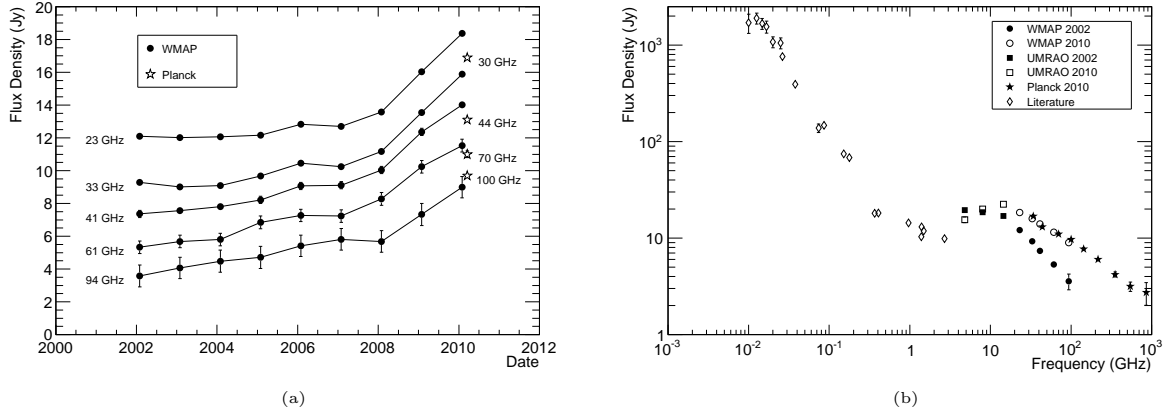


Figure 6. Plots showing a recent yearly-averaged light curve (a) and the radio-to-far-infrared spectral energy distribution (b) for NGC 1275, using data from *WMAP*, *Planck*, UMRAO monitoring, and the literature.

the far-infrared, and that the core has a more pronounced GHz-peaked spectrum, with a peak frequency of ~ 15 GHz in 2010.

The complex changes evident from the multi-frequency properties of NGC 1275 during the last outburst emphasise how vital regular monitoring over a wide frequency range (particularly in the mm/sub-mm) is, if we are to understand the processes that generate this emission. Fortunately over the past decade, the source has been regularly observed as part of the F-GAMMA program (Angelakis et al. 2012) and the Owens Valley Radio Observatory (OVRO) 40 m Telescope Monitoring Program (Richards et al. 2011), and is used as a bright phase calibrator or pointing source at mm/sub-mm wavelengths by the Institut de Radioastronomie Millimétrique (IRAM)’s Plateau de Bure Interferometer (PdBI) (Trippe et al. 2010), the James Clerk Maxwell Telescope (JCMT), the SMA, and the Combined Array for Research in Millimeter-wave Astronomy (CARMA). Therefore, it is very likely that a well-sampled light curve will be available over the 15–350 GHz range to search for any flickering and correlation with the optical and/or γ -ray emission.

To illustrate the potential of combining mm/sub-mm monitoring with the γ -ray emission we compare the SMA 1.3 mm data to the fortnightly- and 3.5-day-binned *Fermi* light curves (Fig. 1 and 2). As stated above, the variations at 1.3 mm do not coincide with the flares in the *Fermi* data. Notwithstanding, we perform a cross-correlation to search for any linear relation between the two datasets displayed in Fig. 1. As the SMA data are unevenly sampled, we use the Discrete Correlation Function (DCF; Edelson & Krolik 1988). The DCF is only applicable to stationary data (e.g. Welsh 1999) so a first-order polynomial was first fitted to, and subtracted from each dataset, in order to remove the long-timescale, rising trend. The DCF for a range of $-1500 < \text{lag} < 1500$ days is shown in Fig. 7. A 30-day DCF bin width was used (it being larger than the mean sampling rate of the γ -ray data of ~ 15 days), giving a minimum of 110 time lag estimates in each bin. To assess the significance of any peaks in the DCF we use the Bartlett formula (Bartlett 1948) to estimate the 95 and 99 per cent confidence

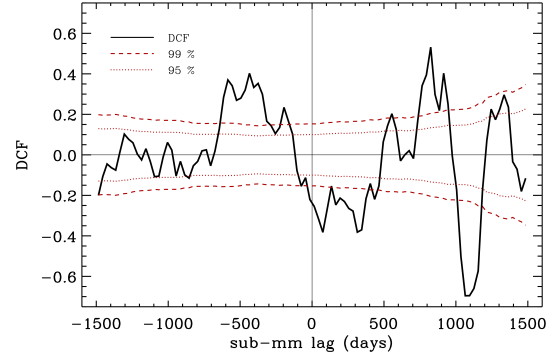


Figure 7. A plot of the DCF produced by cross-correlating the *Fermi* and SMA light curves shown in Fig. 1. The 95 and 99 per cent confidence intervals estimated using the Bartlett formula (Bartlett 1948) are included, though we note that they do not include the effect of uncorrelated coloured noise (e.g. Max-Moerbeck et al. 2013).

intervals, as included in the figure. The most significant features in the data are a positive correlation at $\sim +800$ days, as well as a negative correlation seen at $\sim +1100$ days. A positive correlation is also seen at ~ -450 days. Using a DCF bin size of 100 days, the peaks in the DCF are still present above the 99 per cent level. However, we note that the peaks in the DCF can arise from the underlying shape of uncorrelated coloured-noise light curves (e.g. Alston et al. 2013). Also, removing both the broad, 5-month peak at the end of 2011 from the HE dataset, and the 2-month peak in early 2013 from the SMA dataset causes the sub-mm lag to disappear, which might suggest it is spurious.

The finely-binned light curve illustrated in Fig. 2 is suggestive of significant variability on timescales shorter than the fortnightly binning shown in Fig. 1. The possibility of a flickering nature of the γ -ray emission is an aspect of the source that could be used to determine its structure, and so it was investigated further. We performed chi-square tests with the variously-binned datasets to determine the scale down to which there is evidence of variability. Though we found no evidence for statistically significant variability on the 3.5 day timescale in the *overall* dataset, we found hints

of such during shorter, individual periods. For example, we calculated $\chi^2 = 1.25$ per degree of freedom for the interval illustrated in the middle panel of Fig. 2, implying a chance probability of consistency with the trend observed in the fortnightly-binned data of ~ 1 per cent. It is this period (2010–2012) which contains one of the most prominent flares. It is clear that on the timescales probed in Fig. 2, evidence for variations from one half-a-week to another (that do not simply reflect the variability observed in Fig. 1) begins to emerge in some periods, in spite of poor statistics.

The source of variable high energy γ rays is coincident (within errors), with the nucleus of NGC 1275. Light-crossing-time arguments (which state that emitting regions can only fluctuate over a time less than that taken for light to travel across their extent) mean that any flux variability observed limits the physical size of (at least some component of) the source emission. The detection of a γ -ray flare by *Fermi* on timescales of days to weeks places a firm upper limit on the size of the γ -ray emitting region of less than about 1000 AU. On the other hand, the SMA 1.3 mm monitoring does not show any strong variation on timescales of less than a week, so this emission is either self-absorbed, or from a more extended region. The EGRET upper limit of $F_\gamma < 3.72 \times 10^{-8}$ ph (> 100 MeV) $\text{cm}^{-2}\text{s}^{-1}$ provides a limit on the cluster-scale γ -ray emission of Perseus, which is expected for example from diffuse populations of long-lived CR hadrons (see e.g. Blasi et al. 2007), and in models of dark matter annihilation (e.g. Bringmann & Weniger 2012). Even the lowest flux states evident in Fig. 1 are an order of magnitude above this level.

As mentioned in the introduction, 43 GHz VLBA monitoring of NGC 1275 shows that one component, ‘C3’, accounts for most of the increase in the total flux at this frequency (Nagai et al. 2010; Suzuki et al. 2012; Nagai et al. 2012; The MAGIC Collaboration et al. 2014). If one assumes that C3 is coincident with the nucleus then the evolution of the separation between C1 and C3 presented in Nagai et al. (2010) and Suzuki et al. (2012) can be interpreted as C1 being launched from the nucleus between 2001 and 2003. This coincides with the upturn in activity in the radio and is a more natural explanation than a rapid change in the apparent speed of C3 (Nagai et al. 2010), but implies that the flat spectrum of C1 between 22 and 43 GHz is not due to it being the core as assumed by Suzuki et al. (2012). This indicates that new VLBA components from flaring activity in 2010 and 2011 should become visible in the next couple of years close to C3, and move north if they share the same apparent velocity as C1 relative to the core. Continued VLBA monitoring of NGC 1275 will clarify this issue as it will allow us to link the complex photometric variations to individual resolved knots.

The lack of any significant flux variation in the SMA 1.3 mm light curve during the flares visible in May 2009, August 2010 and September 2011, coupled with the hardening in the *Fermi* flux at these times, strongly suggests that whilst the energy of the electrons in the jet increases and inverse Compton scattering is enhanced during the flaring periods, the overall electron number density (and hence the synchrotron emission) is relatively unchanged. Changes in the electron population; the photons they produce and then up-scatter, depend on the structure of the emission region.

Therefore, variations at one frequency do not necessarily lead to similar variations elsewhere in the spectrum.

Zacharias & Schlickeiser (2013) demonstrate the time-dependent changes seen in the overall SED of a source during and after a flare. There is a significant lag in the X-ray and sub-mm regimes to a flare in the γ rays and optical of days to weeks. This matches the observation that NGC 1275 exhibits enhanced TeV emission in periods of flaring (Aleksić et al. 2012; The MAGIC Collaboration et al. 2014). The Zacharias & Schlickeiser (2013) models suggest emission in the optical and γ rays will show a more direct link in their variability. The simultaneous study of γ -ray and optical variability has only been possible since the launch of *Fermi* and The MAGIC Collaboration et al. (2014) present the first attempt to investigate this: the flux of the two datasets are well correlated. They use optical data from the KVA² optical monitoring, covering the past four years, which confirms that the short-timescale ($< \text{month}$) variation in optical flux visible in the Lyutyi (1977) and Nesterov et al. (1995) results has returned.

Given the rich variety in the variability and relative brightness of NGC 1275, it is to be hoped that it will continue to be monitored at all wavelengths (especially in the optical and TeV), and more frequently over the next few years of increasing activity, to search for direct temporal correlation between the mm/sub-mm, near-infrared, optical and γ -ray emission.

4.3 Wider implications

The variable nature of NGC 1275 has implications for our understanding of other BCGs in cooling-core clusters. It is known that the X-ray emission from BCGs is variable (e.g. Russell et al. 2013) and that a substantial number of GHz-peaked sources are found in BCGs, both with and without additional, steeper-spectrum components (Hogan et al., in preparation), but as yet there have been no systematic searches for radio variability in BCGs in the literature. The example of NGC 1275 is an important one, as it highlights the fact that relying on data from below 10 GHz can overlook the contribution from a synchrotron self-absorbed core.

This is particularly important when considering the contamination of Sunyaev-Zel’dovich (SZ) effect observations in the 30–150 GHz range, where the measured decrement could be underestimated if the additional high-frequency, point source component is not accounted for (see e.g. Knox et al. 2004; Coble et al. 2007; Lin et al. 2009). For instance, the 1.4 GHz flux density for NGC 1275 is comparable to the 100 GHz *Planck* flux density at ~ 10 –12 Jy in 2010 but an extrapolation from the steeper-spectrum emission at lower frequencies would predict a flux of ~ 0.1 Jy. Using NGC 1275 as an example of such a contaminating source, it is clear that having radio data over a broad frequency range and within a few years of the SZ observations is essential to correctly account for this variable, flat-spectrum core emission.

We can also use the observed ratio of radio to γ -ray emission in NGC 1275 to estimate the possible *Fermi* fluxes of other BCGs. Scaling from the 2010 fluxes at 90 GHz and

² <http://users.utu.fi/kani/1m/>

between 0.3–300 GeV of 10 Jy and $3 \times 10^{-8} \text{ ph cm}^{-2} \text{ s}^{-1}$, respectively, the next brightest BCG in the radio band would be 50–100 times fainter in the γ rays, so undetectable at the current *Fermi* exposure level. This agrees with the analysis of Dutson et al. (2013) who considered a sample of 114 core-dominated BCGs and found no individual *Fermi* detections apart from two AGN-dominated sources, already established as HE emitters. Nor was a signal found by co-adding the BCG candidates, so it is uncertain whether it is the proximity of NGC 1275 that makes it exceptional, or that it is in itself peculiar. Its current state is not necessarily typical of the source; continued monitoring decades into the future might address this uncertainty, establishing observationally a complete cycle into and out of an active state. If another moderately bright BCG were to experience an outburst, then *Fermi* ought to be capable of detecting it (particularly during flaring events) but it would require long-term monitoring of dozens of systems at >30 GHz to identify possible candidates.

The properties of NGC 1275 can also inform our understanding of radio galaxies and BL Lac objects. The beaming of the core that makes BL Lacs so prominent also acts to shorten the observed variability timescales at all wavelengths, by an order of magnitude in many cases. Therefore, the outburst timescale observed in NGC 1275 of a few decades with at most *mild* beaming (Nagai et al. 2010), is comparable to the few-year outburst timescale seen in sources such as 3C 279 and 3C 454.3, where the beaming is a factor of order ten higher. Thus, when considering the core dominance of radio galaxies it is important to take into account both the self-absorption of the core, and its potential variability on decade-to-century timescales. The observed properties of NGC 1275 show very little variation below 1 GHz, so selecting a sample of radio galaxies at low frequency (e.g. 159 MHz using the 3C Catalogue; Edge et al. 1959) would select sources like NGC 1275 uniformly, as the level of core activity has little or no effect. However, making the selection at > 15 GHz (e.g. The Australia Telescope 20 GHz Survey; AT20G; Murphy et al. 2010) would depend greatly on when in the last 50 years the object was observed. Ensuring that the ‘time domain’ aspects of the properties of radio galaxies are considered will help build a more self-consistent picture of both beamed and non-beamed radio sources, and the emission mechanisms that give rise to their extraordinary multiwavelength properties.

5 CONCLUDING REMARKS

NGC 1275 has been pivotal to our understanding of AGN feedback over the past three decades (see e.g. Böhringer et al. 1993; Fabian et al. 2000). The presence of multiple ‘bubbles’ in the intracluster medium of the surrounding cluster indicates that there are major outbursts from the core on timescales of 10^{6-7} years.

Building on previous work, this paper provides striking evidence for variability of NGC 1275 on decade timescales, showing that there are repeated outbursts from the central few parsecs of the source, which vary in amplitude by about an order of magnitude. On top of this episodic variability there is also short-timescale flaring activity seen over a few days to a month in the γ rays, that can produce an additional

order-of-magnitude brightening in flux and coincide with a detection at TeV energies.

NGC 1275 is currently brightening rapidly and may reach a luminosity similar to that observed for over a decade in the 1960’s and 1970’s. The much broader range of multi-wavelength facilities available now will present an unprecedented opportunity to study the behaviour of the source during a very active phase. In particular, linking the shorter-timescale γ -ray variability to the launching of individual radio components in the jet (e.g. Suzuki et al. 2012) is now possible with continued monitoring with long baseline interferometers at high frequency (>20 GHz). Therefore, the current outburst will provide us with an opportunity to witness processes at the very heart of AGN feedback.

ACKNOWLEDGEMENTS

The SMA is a joint project between the Smithsonian Astrophysical Observatory and the Academia Sinica Institute of Astronomy and Astrophysics, and is funded by the Smithsonian Institution and the Academia Sinica. This work has made use of public *Fermi* data and Science Tools provided by the *Fermi* Science Support Centre, the NASA/IPAC Extragalactic Database (NED) which is operated by the Jet Propulsion Laboratory, California Institute of Technology, under contract with NASA, and the SIMBAD and VIZIER databases, operated at CDS, Strasbourg, France. We thank Margo Aller for permission to use data from the University of Michigan Radio Astronomy Observatory, which was supported by the National Science Foundation and NASA, and by funds from the University of Michigan. We thank also Richard White, whose automated *Fermi* tool chain improved the time-efficiency of much of the analysis carried out. K. L. Dutson acknowledges support from the STFC studentship ST/I505780/1 and the STFC Doctoral Training Grant ST/J501104/1, M. T. Hogan from the STFC studentship ST/I505656/1, W. N. Alston from the EU FP7-SPACE research project, STRONGGRAVITY., J. A. Hinton from the Leverhulme Trust, and A. C. Edge from STFC grant ST/I001573/1.

REFERENCES

- Abdo A. A., et al., 2009, *ApJ*, 699, 31
- Ackermann M., et al., 2012, *ApJS*, 203, 4
- Aleksić J., et al., 2012, *A&A*, 539, L2
- Aller H. D., Aller M. F., Latimer G. E., Hodge P. E., 1985, *ApJS*, 59, 513
- Alston W. N., Vaughan S., Uttley P., 2013, *MNRAS*, 429, 75
- Angelakis E., Fuhrmann L., Nestoras I., Fromm C. M., Perucho-Pla M., Schmidt R., Zensus J. A., Marchili N., Krichbaum T. P., Ungerechts H., Sievers A., Riquelme D., Pavlidou V., 2012, *Journal of Physics Conference Series*, 372, 012007
- Atwood W. B., et al., 2009, *ApJ*, 697, 1071
- Bartlett M. S., 1948, *Nature*, 161, 686
- Barvainis R., Predmore C. R., 1984, *ApJ*, 282, 402
- Bignami G. F., Boella G., Burger J. J., Taylor B. G., Keirle P., Paul J. A., Mayer-Hasselwander H. A., Pfeffermann E.,

- Scarsi L., Swanenburg B. N., 1975, *Space Science Instrumentation*, 1, 245
- Blasi P., Gabici S., Brunetti G., 2007, *IJMPA*, 22, 681
- Böhringer H., Voges W., Fabian A. C., Edge A. C., Neumann D. M., 1993, *MNRAS*, 264, L25
- Bower R. G., Benson A. J., Malbon R., Helly J. C., Frenk C. S., Baugh C. M., Cole S., Lacey C. G., 2006, *MNRAS*, 370, 645
- Bringmann T., Weniger C., 2012, *Dark Universe*, 1, 194
- Brown M., Adams J., 2012, *MNRAS*, 413, 2785
- Coble K., Bonamente M., Carlstrom J. E., Dawson K., Hasler N., Holzappel W., Joy M., La Roque S., Marrone D. P., Reese E. D., 2007, *AJ*, 134, 897
- Conselice C. J., Gallagher J. S., Wyse R. F. G., 2001, *ApJ*, 122, 2281
- Croton D. J., Springel V., White S. D. M., De Lucia G., Frenk C. S., Gao L., Jenkins A., Kauffmann G., Navarro J. F., Yoshida N., 2006, *MNRAS*, 365, 11
- Dunn R. J. H., Fabian A. C., Sanders J. S., 2006, *MNRAS*, 366, 758
- Dutson K. L., White R. J., Edge A. C., Hinton J. A., Hogan M. T., 2013, *MNRAS*, 429, 2069
- Edelson R. A., Krolik J. H., 1988, *ApJ*, 333, 646
- Edge D. O., Shakeshaft J. R., McAdam W. B., Baldwin J. E., Archer S., 1959, *Mem. R. Astron. Soc.*, 68, 37
- Epstein E. E., Pomphrey R. B., Fogarty W. G., 1979, *Publ. Astron. Soc. Pac.*, 91, 163
- Fabian A., 2001, in *Chandra Proposal A DETAILED STUDY OF THE CORE OF THE PERSEUS CLUSTER*. p. 988
- Fabian A. C., 1994, *Annu. Rev. Astron. Astrophys.*, 32, 277
- Fabian A. C., 2012, *Annu. Rev. Astron. Astrophys.*, 50, 455
- Fabian A. C., Sanders J. S., Allen S. W., Crawford C. S., Iwasawa K., Johnstone R. M., Schmidt R. W., Taylor G. B., 2003, *MNRAS*, 344, L43
- Fabian A. C., Sanders J. S., Crawford C. S., Conselice C. J., Gallagher J. S. I., Wyse R. F. G., 2003, *MNRAS*, 344, L48
- Fabian A. C., Sanders J. S., Ettori S., Taylor G. B., Allen S. W., Crawford C. S., Iwasawa K., Johnstone R. M., Ogle P. M., 2000, *MNRAS*, 318, L65
- Falceto-Gonçalves D., Caproni A., Abraham Z., Teixeira D. M., de Gouveia Dal Pino E. M., 2010, *ApJ*, 713, L74
- Flett A. M., Henderson C., 1981, *MNRAS*, 194, 961
- Flett A. M., Henderson C., 1983, *MNRAS*, 204, 1285
- Fogarty W. G., Epstein E. E., Montgomery J. W., Dworetzsky M. M., 1971, *AJ*, 76, 537
- Gitti M., Brunetti G., Setti G., 2002, *A&A*, 386, 456
- Gurwell M. A., Peck A. B., Hostler S. R., Darrah M. R., Katz C. A., 2007, in *Baker A. J., Glenn J., Harris A. I., Mangum J. G., Yun M. S., eds, From Z-Machines to ALMA: (Sub)Millimeter Spectroscopy of Galaxies MONITORING PHASE CALIBRATORS AT SUBMILLIMETER WAVELENGTHS*. p. 234
- Hobbs R. W., Corbett H. H., Santini N. J., 1969, *ApJL*, 156, L15
- Kataoka J., et al., 2010, *ApJ*, 715, 554
- Kingham K. A., Oconnell R. W., 1979, *AJ*, 84, 1537
- Knox L., Holder G. P., Church S. E., 2004, *ApJ*, 612, 96
- Krichbaum T. P., et al., 1992, *A&A*, 260, 33
- Landau R., Epstein E. E., Rather J. D. G., 1980, *AJ*, 85, 363
- Lin Y.-T., Partridge B., Pober J. C., Boucheffry K. E., Burke S., Klein J. N., Coish J. W., Huffenberger K. M., 2009, *ApJ*, 694, 992
- Lyuty V. M., 1977, *SvA*, 21, 655
- Mattox J. R., et al., 1996, *ApJ*, 461, 396
- Max-Moerbeck W., Richards J. L., Pavlidou V., Pearson T. J., Readhead A. C. S., on behalf of the Fermi LAT collaboration Hovatta T., King O. G., Reeves R., 2013, *ArXiv e-prints*
- McNamara B. R., Nulsen P. E. J., 2012, *New Journal of Physics*, 14, 055023
- Murphy T., et al., 2010, *MNRAS*, 402, 2403
- Nagai H., Orienti M., Kino M., Suzuki K., Giovannini G., Doi A., Asada K., Giroletti M., Kataoka J., D'Ammando F., Inoue M., Lähteenmäki A., Tornikoski M., León-Tavares J., Kamenno S., Bach U., 2012, *MNRAS*, 423, L122
- Nagai H., Suzuki K., Asada K., Kino M., Kamenno S., Doi A., Inoue M., Kataoka J., Bach U., Hirota T., Matsumoto N., Honma M., Kobayashi H., Fujisawa K., 2010, *PASJ*, 62, L11
- Nesterov N. S., Lyuty V. M., Valtaoja E., 1995, *A&A*, 296, 628
- Nolan P. L., et al., 2012, *ApJS*, 199, 31
- O'Dea C. P., Dent W. A., Balonek T. J., 1984, *ApJ*, 278, 89
- Planck Collaboration Ade P. A. R., Aghanim N., Arnaud M., Ashdown M., Aumont J., Baccigalupi C., Balbi A., Banday A. J., Barreiro R. B., et al. 2011, *A&A*, 536, A7
- Reimer O., Pohl M., Sreekumar P., Mattox J. R., 2003, *ApJ*, 588, 155
- Reuter H.-P., Kramer C., Sievers A., Paubert G., Moreno R., Greve A., Leon S., Panis J. F., Ruiz-Moreno M., Ungerechts H., Wild W., 1997, *A&As*, 122, 271
- Richards J. L., et al., 2011, *ApJS*, 194, 29
- Russell H. R., McNamara B. R., Edge A. C., Hogan M. T., Main R. A., Vantyghem A. N., 2013, *MNRAS*, 432, 530
- Salomé P., et al., 2006, *A&A*, 454, 437
- Schorn R. A., Epstein E. E., Oliver J. P., Soter S. L., Wilson W. J., 1968, *ApJL*, 151, L27
- Steppe H., Paubert G., Sievers A., Reuter H. P., Greve A., Liechti S., Le Floch B., Brunswig W., Menendez C., Sanchez S., 1993, *A&As*, 102, 611
- Strong A. W., Bignami G. F., 1983, *ApJ*, 274, 549
- Suzuki K., Nagai H., Kino M., Kataoka J., Asada K., Doi A., Inoue M., Orienti M., Giovannini G., Giroletti M., Lähteenmäki A., Tornikoski M., León-Tavares J., Bach U., Kamenno S., Kobayashi H., 2012, *ApJ*, 746, 140
- The MAGIC Collaboration et al., 2014, 564, A5
- Trippe S., Krips M., Piétu V., Neri R., Winters J. M., Gueth F., Bremer M., Salome P., Moreno R., Boissier J., Fontani F., 2011, *A&A*, 533, A97
- Trippe S., Neri R., Krips M., Castro-Carrizo A., Bremer M., Piétu V., Fontana A. L., 2010, *A&A*, 515, A40
- Welsh W. F., 1999, *Publ. Astron. Soc. Pac.*, 111, 1347
- Wilman R. J., Edge A. C., Johnstone R. M., 2005, *MNRAS*, 359, 755
- Wright E. L., et al., 2009, *ApJS*, 180, 283
- Zacharias M., Schlickeiser R., 2013, *ApJ*, 777, 109

This paper has been typeset from a \LaTeX file prepared by the author.